Available online at www.sciencedirect.com
ScienceDirect
Nuclear Instruments and Methods in Physics Research B 266 (2008) 425–434
NIM B
Beam Interactions with Materials & Atoms
www.elsevier.com/locate/nimb

Correlation–polarization effects in electron/positron scattering from acetylene: A comparison of computational models

J. Franz [a], F.A. Gianturco [b,*], K.L. Baluja [c], J. Tennyson [a], R. Carey [d], R. Montuoro [d], R.R. Lucchese [d], T. Stoecklin [e], P. Nicholas [f], T.L. Gibson [f]

[a] Department of Physics and Astronomy, University College London, Gower Street, London WC1E 6BT, United Kingdom
[b] Department of Chemistry, The University of Rome La Sapienza and CNISM, Piazzale A. Moro 5, 00185 Rome, Italy
[c] Department of Physics and Astrophysics, University of Delhi, Delhi 110 007, India
[d] Department of Chemistry, Texas A&M University, College Station, TX 77843-3255, USA
[e] Institut des Sciences Moléculaires, CNRS-UMR 5255, 351 Cours de la Libération, F-33405 Talence, France
[f] Department of Physics, Texas Tech University, P.O. Box 4180, Lubbock, Texas, 79409-1051, USA

Available online 15 December 2007

Abstract

Different computational methods are employed to evaluate elastic (rotationally summed) integral and differential cross sections for low energy (below about 10 eV) positron scattering off gas-phase C_2H_2 molecules. The computations are carried out at the static and static-plus-polarization levels for describing the interaction forces and the correlation–polarization contributions are found to be an essential component for the correct description of low-energy cross section behavior. The local model potentials derived from density functional theory (DFT) and from the distributed positron model (DPM) are found to produce very high-quality agreement with existing measurements. On the other hand, the less satisfactory agreement between the R-matrix (RM) results and measured data shows the effects of the slow convergence rate of configuration-interaction (CI) expansion methods with respect to the size of the CI-expansion. To contrast the positron scattering findings, results for electron–C_2H_2 integral and differential cross sections, calculated with both a DFT model potential and the R-matrix method, are compared and analysed around the shape resonance energy region and found to produce better internal agreement.

PACS: 31.25.v; 34.80.Bm; 34.85.+x

Keywords: Electron–molecule scattering; Positron–molecule scattering; Computed angular distributions for e^+/e^- scattering; Quantum calculations; Molecular gases

1. Introduction

The increase of interest in high-quality measurements involving antimatter has attracted,in recent years, the attention of experimentalists and theoreticians in the field of molecular physics [1–5]. This has generated a wealth of new information on the nanoscopic behavior of a broad variety of molecular systems when they are made to interact with beams of positrons at thermal and near-thermal energies. To understand the interaction of positron beams with matter, it becomes important to also be able to distinguish to what extent the additional features of positron interaction with molecules (e.g. Ps formation and positron annihilation) are related to positron dynamics and to positron–electron correlation features. The study of even the simplest of such observables, e.g. the elastic scattering integral and differential cross sections occurring below the thresholds of Positroniun (Ps) formation in polyatomic gases, already provides a very useful testing ground for the theoretical and computational models which are currently employed to analyze positron-matter dynamics [2].

While the electrostatic interaction can in principle be described exactly by an essentially repulsive potential due

* Corresponding author. Fax: +39 06 4991 3305.
E-mail address: fa.gianturco@caspur.it (F.A. Gianturco).

0168-583X/$ - see front matter © 2007 Elsevier B.V. All rights reserved.
doi:10.1016/j.nimb.2007.12.019

to the molecular network of (electrons + nuclei), different approximations for correlation–polarization effects – the V_{pcp} potential – play an essential role in deciding the quality of the adopted theoretical model over the whole range of relevant distances between target and the positron projectile. As the projectile nears the target, in fact, the repulsive Coulombic core further slows it down while the attraction from the bound electrons increases and strongly modifies its motion in the intermediate range of distances via a correlation mechanism reminiscent of multiple scattering effects [6]. This short-range effect should therefore be energy-dependent and nonlocal and would asymptotically give rise to charge-induced polarization effects, the leading term of which will be given via the dipole-polarizability of the target molecule [6]. The evaluation of the V_{pcp} contribution to positron–molecule interaction is therefore central to theoretical scattering calculations and its correct evaluation within cross section modelling studies is one of the stumbling blocks to the quantitative interpretation of existing experimental findings.

In the present paper we therefore carry out a detailed comparison of the results of different theoretical approximations for the correlation–polarization forces by using the acetylene molecule as a benchmark system, in view of the availability of good quality experimental data on this system and of its relatively simple structure as a polyatomic target.

The structure of the paper shall be the following: in the next Section 2 we will report in some detail an outline of the methods employed to generate correlation–polarization and static potentials while Section 3 will give and discuss our results for the elastic (rotationally summed) integral cross sections. The differential cross sections will also be given by Section 3, while our conclusions will be collected in Section 4.

2. Scattering equations and interaction forces

In order to carry out our comparison between different treatments of correlation–polarization forces, we have tested three different approaches: we have employed the single-center-expansion (SCE) treatment of the scattering problem and included the V_{pcp} potential in two different ways, i.e. the Density functional modelling (DFT), used by us before [7] and the distributed positron model (DPM) also introduced earlier on [8] and employed within the SCE treatment. We have then tested a configuration interaction (CI) procedure and implemented it within the R-matrix (RM) treatment of the scattering process [9]. Comparison with calculations by other groups [10] will also be given for the sake of completeness. In the following we shall provide a short outline of each of the above computational methods.

2.1. The SCE scattering equations

In order to obtain the scattering cross sections for polyatomic molecules, we need to solve the Schrodinger equation for the total system

$$(H - E)\Psi = 0 \tag{1}$$

at the total energy E, for the corresponding wavefunction Ψ. Here H is the total Hamiltonian given by

$$H = \hat{H}_{mol} + \hat{K} + \hat{V}, \tag{2}$$

where $\hat{H}_{mol}, \hat{K}$ and $\hat{V}$ represent the operators of the molecular Hamiltonian, kinetic energy of the scattered positron and interaction between the incident positron and the target molecule, respectively. The $\hat{H}_{mol}$ further consists, in general, of the rotational and vibrational parts

$$H_{mol} = H_{rot} + H_{vib}, \tag{3}$$

whereby we exclude, at the collision energies considered, both electronic excitations and the Ps formation channels.

The total wavefunction Ψ described in the molecular frame (MF) reference system in which the z-axis is taken along the direction of the main molecular axis, is expanded around a single-centre (SCE) as

$$\Psi(\mathbf{r}_1 \ldots \mathbf{r}_Z, \mathbf{r}_p|\mathbf{R}) = \Psi_{mol}(\mathbf{r}_1 \ldots \mathbf{r}_Z|\mathbf{R})\varphi(\mathbf{r}_p|\mathbf{R}), \tag{4}$$

where

$$\varphi(\mathbf{r}_p|\mathbf{R}) = \sum_{l\pi\mu h} r_p^{-1} u_{lh}^{\pi\mu}(r_p|\mathbf{R}) X_{hl}^{\pi\mu}(\hat{\mathbf{r}}_p). \tag{5}$$

In Eq. (4), $\mathbf{r_i}$ represents the position vector of the ith electron among the Z bound electrons of the target, taken from the center of mass. The quantity Ψ_{mol} represents the electronic wavefunction for the molecular target at the nuclear geometry $\mathbf{R}$. The continuum function $\varphi(\mathbf{r_p}|\mathbf{R})$ refers to the wavefunction of the scattered positron under the full action of the field created by the molecular electrons and by their response to the impinging positron as described below. Each $u_{lh}^{\pi\mu}$ is the radial part of the wavefunction for the incident particle and the $X_{hl}^{\pi\mu}$ are the symmetry-adapted angular basis functions discussed earlier [11] which we will not repeat further here.

The label π stands for the irreducible representation (IR), μ distinguishes the components of the basis for each IR and $\{\pi l\}$, respectively.

Since the molecular rotations and vibrations are often slow when compared with the velocity of the impinging positrons considered in the present study, we may apply the fixed-nuclei (FN) approximation [12] that ignores the molecular term of H_{mol} in Eq. (2) and fixes the values of all $\mathbf{R}$ at their equilibrium locations in each of the target molecules. We then solve the Schrödinger equation in the FN approximation, make use of the MF system rather than the space-frame (SF) reference system: the two systems are related through a frame transformation scheme given, for example, by [12].

After substituting Eq. (4) into (1) under the FN approximation, we obtain a set of coupled differential equations for u_{lv} where, for simplicity, v represents $(\pi\mu h)$ collectively:

$$\left\{\frac{\mathrm{d}^2}{\mathrm{d}r_\mathrm{p}^2}-\frac{l(l+1)}{r_\mathrm{p}^2}+k^2\right\}u_{lv}(r_\mathrm{p}|\mathbf{R}) = 2\sum_{l'v'}\langle lv|\mathbf{V}|l'v'\rangle u_{l'v'}(r_\mathrm{p}|\mathbf{R}) \quad (6)$$

with

$$\langle lv|\mathbf{V}|l'v'\rangle = \int \mathrm{d}\hat{r}_\mathrm{p} X_{lv}(\hat{r}_\mathrm{p}) * V(r_\mathrm{p}|\mathbf{R}) X_{l'v'}(\hat{r}_\mathrm{p}). \quad (7)$$

Solving Eq. (6) under the boundary conditions that the asymptotic form of $u^{lv}_{l'v'}$ is represented by a sum containing the incident plane wave of the projectile and the outgoing spherical wave we obtain the corresponding S-matrix elements, $S^{lv}_{l'v'}$. The actual numerical procedure we have employed to solve that equation was given in detail in [13,14].

After transforming the MF quantities into the SF frame, the integral cross section (ICS) for the elastic scattering, rotationally summed over molecular rotations, is given by

$$Q = \frac{\pi}{k^2}\sum_{lv}\sum_{l'v'}|T^{lv}_{l'v'}|^2, \quad (8)$$

where $T^{lv}_{l'v'} = \delta_{ll'}\delta_{vv'} - S^{lv}_{l'v'}$.

2.2. The DFT modelling of correlation–polarization

The present treatment of the short-range part of the full V_pcp interaction was first applied to positron scattering problems by some of the authors [7] and is based on constructing the correlation energy $\varepsilon^{\mathrm{e-p}}$ of a localized positron in an electron gas and in further connecting it with the correct asymptotic form of the spherical dipole polarizability component contained within the full potential reported on the RHS of Eq. (6). The quantity $\varepsilon^{\mathrm{e-p}}$ had been originally derived by Arponen and Pajanne [15] by assuming that the incoming positron can be treated as a charged impurity at a fixed distance r_p in an homogeneous electron gas, which is in turn described as a set of interacting bosons representing the collective excitations within the random phase approximation. Based on their work, Boronski and Nieminen [16] have given the interpolation formulae of $\varepsilon^{\mathrm{e-p}}$ over the entire range of the density parameter r_s, which satisfies the relationship $\frac{4}{3}\pi r_\mathrm{s}^3\rho(\mathbf{r}) = 1$, with $\rho(\mathbf{r})$ being the density of the Z bound electrons.

The relationship between the correlation potential V_corr and $\varepsilon^{\mathrm{e-p}}$, which is consistent with the local density approximation and a variational principle for a total collision system with the size of the target, is given by the functional derivative of $\varepsilon^{\mathrm{e-p}}$ with respect to the electron density in the target:

$$V_\mathrm{corr}(\mathbf{r}_\mathrm{p}|\mathbf{R}) = \frac{\delta}{\delta\rho}\{\varepsilon^{\mathrm{e-p}}[\rho(\mathbf{r}_\mathrm{e}|\mathbf{R})]\}, \quad (9)$$

where in our treatment $\rho(\mathbf{r}_\mathrm{e}|\mathbf{R})$ denotes the undistorted electronic density of the target, obtained from accurate Hartree-Fock (HF) calculations, as a function of the molecular geometry and the r_e coordinates of the bound electrons. This quantity provides the probability of finding any of the molecular electrons near the impinging positron once an analytic ansatz is provided for $\varepsilon^{\mathrm{e-p}}$ [16]. Thus, the total V_pcp potential for the e^+–molecule system can be assembled by writing, for each molecular geometry.

$$V_\mathrm{pcp}(\mathbf{r}_\mathrm{p}|\mathbf{R}) = \begin{cases} V_\mathrm{corr}(\mathbf{r}_\mathrm{p}|R) & \text{for} \quad \mathbf{r}_\mathrm{p} < r_\mathrm{c} \\ V_\mathrm{pol}(\mathbf{r}_\mathrm{p}|R) & \text{for} \quad \mathbf{r}_\mathrm{p} > r_\mathrm{c} \end{cases}. \quad (10)$$

The V_corr is connected to the spherical part of the asymptotic form of the polarization at the position of r_c, usually around 4.0 a_u for our systems. It corresponds to the outer crossing between the potential contributions of Eq. (10).

The total interaction potential V_tot is therefore given by the exact static interaction V_st between the impinging positron and the components (electrons and nuclei) of the molecular target, (for its detailed form see, for example, [7]) plus the V_pcp given by equation [10] for each choice of fixed molecular geometry $\mathbf{R}$:

$$V_\mathrm{tot}(\mathbf{r}_\mathrm{p}|\mathbf{R}) = V_\mathrm{st}(\mathbf{r}_\mathrm{p}|\mathbf{R}) + V_\mathrm{pcp}(\mathbf{r}_\mathrm{p}|\mathbf{R}). \quad (11)$$

2.3. The distributed positron model

An alternative model correlation–polarization potential we have used to describe the V_pcp in Eq. (10) is the distributed positron model (DPM) potential, $V^\mathrm{DPM}_\mathrm{pcp}$ [17,18]. The form adopted here for the correlation–polarization $V^\mathrm{DPM}_\mathrm{pcp}$ is based on a modification of the adiabatic polarization approximation, which provides a variational estimate of the polarization potential. In the adiabatic polarization approximation, in fact, the positron is treated as an additional "nucleus" (a point charge of +1) fixed at location r_p with respect to the center of mass of the atomic or molecular target. The target orbitals are allowed to relax in the presence of this fixed additional charge and the decrease in energy due to the distortion is recorded. The difference between the final and initial values of the energy defines the adiabatic polarization potential at one point in space. In order to describe carefully the spatial dependence of this interaction, the calculations need to be performed on a rather large number of three dimensional grid points.

However, due to nonadiabatic and short-range correlation effects, e.g. virtual Ps formation, the adiabatic approximation may overestimate the strength of the polarization potential for smaller values of r_p, where the positron has penetrated the target electronic cloud. The present model corrects for this by treating the positron as a "smeared out" charge distribution rather than as a point charge. If the scattering particle really were an additional point charge, then the dominant short-range correlation effect would be virtual hydrogen atom formation into ground and excited states and the δ-function distribution of positive charge at the center of mass would be correct. But, for a Ps atom, the positive charge is not localized at the center of mass and to mimic this effect in computing the polarization potential we represent the positron as a spherically symmetric distribution of charge. This leads to a

polarization potential that more closely reflects the correct physics and that smoothly reduces to the expected result for larger values of r_p without any need to select a cross-over distance as done in the previous treatment.

Within the above model, one can, in principle, choose any reasonable distribution that approximates the positive charge for virtual Ps embedded in the near-target environment. Studies by Gibson [17] have shown that constructing the positron charge distribution from the 1s STO-3G basis function with the tighter Slater exponent of $\xi = 1.24$ as recommended [18–21] for a molecular environment leads to accurate results. Once the $V_{\mathrm{pcp}}^{\mathrm{DPM}}$ potential is calculated, it is combined with the static potential to yield the total local interaction potential of Eq. (10).

After the development of the DPM to account for nonadiabatic polarization effects in positron–molecule scattering, a somewhat similar scheme was proposed by Bouferguene et al. [22] for low-energy electron–H_2 collisions in which the polarization interaction is computed by replacing the impinging electron with a spherical Gaussian distribution of charge -1. Like the DPM for positron scattering, this has the effect of reducing the overestimation of the adiabatic potential near the target and can be very efficiently implemented within a quantum chemistry framework. However, for electron scattering these authors [22] found it necessary to use a distribution that varies with the distance of the scattering electron from the molecular center of mass and involves a semi-empirical parameter.

In contrast, we have been able to obtain good agreement with various measured positron–molecule scattering results within the DPM using essentially the same procedure (i.e. without needing to adjust for details of the target molecule) on a variety of systems [17–20] as diverse as H_2 and SF_6. This past success is the chief motivation for including the DPM in the current study. In conclusion we construct the charge distribution from a 1s STO-3G basis function with Slater exponent $\xi = 1.24$ and once the $V_{\mathrm{pcp}}^{\mathrm{DPM}}$ potential is calculated, it is combined with the static potential to yield the total local interaction potential of Eq. (10), as mentioned before [23].

2.4. The ab initio R-matrix approach for e^+/e^- scattering

In the R-matrix method the space is divided into two regions: an inner region, defined by a sphere typically of radius 10–15a_0 and an outer region. In the inner region the complicated many-particle problem with correlation and polarization effects has to be solved. In the outer region the target is represented by a multipole expansion and the one-particle problem is solved by propagating the R-matrix outwards. The R-matrix provides the link between the two regions.

For molecular targets, the calculations within the inner region reduce to a modified electronic structure calculation and standard quantum chemistry codes have been adapted to this purpose. In particular the UK molecular R-matrix codes [27] use adapted versions [28,29] of the Alchemy and Sweden-Molecule codes for diatomic and polyatomic targets, respectively. All calculations discussed here employ updated versions of these codes. For diatomic targets an implementation for positron scattering was made some time ago [30,31] and has recently been extended to polyatomic targets [32].

The scattering wavefunction for a given energy E is built up as a linear combination [27]

$$\Psi(E) = \sum_k A_K(E)\Psi_K, \tag{12}$$

where the coefficients A_K are obtained by propagating the R-matrix into the outer region. The R-matrix basis functions are represented by the close-coupling expansion [9]

$$\Psi_K = \sum_A \sum_i b_{Ai}^K \hat{\mathscr{A}}(\Xi_A^{Ne}\eta_i) + \sum_B \sum_r c_{Br}^K \Phi_{Br}^{N+1}, \tag{13}$$

where the first sum runs over all products of target wavefunctions Ξ_A^{Ne} and electronic continuum orbitals $\eta_{\bar{x}}$ and $\hat{\mathscr{A}}$ antisymmetrizes all electrons. The second sum runs over square-integrable functions Φ_{Br}^{Z+1} of $(Z+1)$ particles. In the following we shortly describe the three different types of basis functions. The target wavefunction Ξ_A^{Ne} are obtained by diagonalizing the Hamiltonian for the target molecule containing N electrons. In general the eigenfunctions of the target hamiltonian are linear combinations of Slater determinants Λ_D^{Ne}. In the scattering calculations the target functions are multiplied by the continuum orbitals $\eta_i(\mathbf{r}_{Z+1})$ which are occupied by the scattered particle

$$\hat{\mathscr{A}}(\Xi_A^{Ne}\eta_i) = \sum_D d_D^A \hat{\mathscr{A}}(\Lambda_D^{Ne}(\mathbf{r}_1,\cdots,\mathbf{r}_Z)\times\eta_i(\mathbf{r}_{Z+1})). \tag{14}$$

Here the antisymmetrizer $\hat{\mathscr{A}}$ acts only on the electrons. Therefore in electron–molecule scattering calculations the continuum orbital is anti-symmetrized with the target wavefunctions, whereas in positron–molecule scattering calculations the extra orbital is simply multiplied with the target wavefunction. In both cases the coefficients d_D^A are kept fixed (see e.g. [33] for an efficient algorithm). The square-integrable functions are given by

$$\begin{aligned}\Phi_{Br}^{Z+1} &= \Phi_{Br}^{N+1}(\mathbf{r}_1,\ldots,\mathbf{r}_Z,\mathbf{r}_{Z+1}) \\ &= \hat{\mathscr{A}}(\Lambda_B^{Ne}(\mathbf{r}_1,\ldots,\mathbf{r}_Z)\times\chi_r(\mathbf{r}_{Z+1})),\end{aligned} \tag{15}$$

where Λ_B^{Ne} is a N electron function, like a Slater determinant and $\chi_r(\mathbf{r}_{Z+1})$ is a square-integrable spin-orbital. In the case of electron scattering the latter one is anti-symmetrized with the former orbitals.

For electron scattering we have applied the static-exchange (SE) model and the static-exchange-plus-polarization (SEP) model. In both models the target is described by a Hartree-Fock wavefunction. In the SE model the additional electron can occupy all virtual orbitals as well as a set of single centered diffuse Gaussian orbitals which are used to represent the continuum within the R-matrix sphere[35]. In the SEP model all single excitations are added to the configurations generated in the SE model.

In the case of positron scattering we use the same spatial orbitals for both electrons and positrons and define both a static and a static-plus-polarization (SP) model in analogy with the SE and SEP models employed for electron scattering. However, the positron can occupy all orbitals, including those orbitals, which are occupied by electrons. Furthermore, different spin-coupling rules apply in the two cases since the positron spin is not coupled with the bound electron spins.

2.5. Semi-empirical R-matrix approach using an enhancement-factor

In order to model correlation effects which are not fully described in the SP model, we have experimented with scaling the electron–positron attraction integrals by an empirically adjusted enhancement factor, f. These integrals are the ones which are routinely referred to as two-electron integrals in standard quantum chemistry language. Here we wish to only increase the electron–positron attraction so do not alter the corresponding electron–electron integrals.

$$(pq|\overline{rs})_{\mathrm{enh}} = f(pq|\overline{rs}), \tag{16}$$

$$= f\int \phi_{\mathrm{p}}(\mathbf{r}_1)\phi_q(\mathbf{r}_1)\left(-\frac{1}{|r_{1\bar{1}}|}\right)\overline{\chi_r}(\mathbf{r}_{\bar{1}})\overline{\chi_s}(\mathbf{r}_{\bar{1}})d\mathbf{r}_1 d\mathbf{r}_{\bar{1}}. \tag{17}$$

Here $\phi_p(\mathbf{r}_1)$ and $\phi_q(\mathbf{r}_1)$ are electron orbitals, $\overline{\chi_r}(\mathbf{r}_{\bar{1}})$ and $\overline{\chi_s}(\mathbf{r}_{\bar{1}})$ are positron orbitals and $|r_{1\bar{1}}| = |\mathbf{r}_1 - \mathbf{r}_{\bar{1}}|$ is the electron–positron distance.

This form of scaling can be justified as follows. The second order contribution of a Møller-Plesset type perturbative expansion of the electron–positron correlation energy [36] is given by

$$E^{(2)} = \sum_{ia\bar{i}\bar{a}} \frac{(ia|\bar{i}\bar{a})^2}{\epsilon_i - \epsilon_a + \epsilon_{\bar{i}} - \epsilon_{\bar{a}}} = \sum_{i\bar{i}} (ii|\overline{ii})^{(2)}. \tag{18}$$

Here ϵ_i and ϵ_a denote energies of occupied and virtual electronic orbitals, respectively. $\epsilon_{\bar{i}}$ and $\epsilon_{\bar{a}}$ are the same for positrons. Here we have introduced a second-order correction $(ii|\overline{ii})^{(2)}$ to the electron–positron attraction integral $(ii|\overline{ii})$. Since all denominators in the above expression are negative, this correction is always negative and therefore has the same sign the integral $(ii|\overline{ii})$ itself. By defining the pair-dependent enhancement factor

$$f_{i\bar{i}} = 1 + \frac{(ii|\overline{ii})^{(2)}}{(ii|\overline{ii})}, \tag{19}$$

the sum of first- and second-order contributions can be re-expressed as

$$E^{(1+2)} = \sum_{i\bar{i}} (ii|\overline{ii}) + \sum_{i\bar{i}} (ii|\overline{ii})^{(2)} = \sum_{i\bar{i}} f_{i\bar{i}}(ii|\overline{ii}). \tag{20}$$

If we assume, that the enhancement is the same for each electron–positron pair, we can replace the pair-dependent enhancement factor $f_{i\bar{i}}^{(2)}$ by an averaged enhancement factor f

$$E^{(1+2)} \approx \sum_{i\bar{i}} f(ii|\overline{ii}), \tag{21}$$

as used in this paper. In our computations we have used integrals of the more general type $(ij|\overline{ij})$, for which the second-order correction might be positive, resulting in enhancement factors smaller than one. We have however used the same enhancement factor for all integral types.

For large distances r_{p} between the positron and the scattering center the second-order contribution to the electron–positron correlation energy goes over to the asymptotic polarization potential which is given by (in a.u.) [37]

$$-\frac{\alpha_0}{2r_{\mathrm{p}}^4} - P_2(\cos\theta)\frac{\alpha_2}{2r_{\mathrm{p}}^4} \tag{22}$$

for a linear molecule. Here α_0 (α_2) is the spherical (anisotropic) polarizability of the target molecule and $P_2(\cos\theta)$ is a Legendre polynomial, where θ is the angle between the vector linking the positron to the molecular centre-of-mass and that of the molecule. The long-range polarization is included automatically, if not completely, in calculations which use coupled-state expansions [38,39] but not in the SP model. Below we also discuss the influence of including asymptotic polarization potential outside the R-matrix box, something that was also tested in earlier R-matrix studies of positron–molecule collisions [31,40]. In this paper the asymptotic polarization potential has been neglected outside the R-matrix box. This effect has been studied in more detail in [34]. In all calculations the quadrupole moment generated by the target molecule was included in the outer-region.

The present approach is related, but not equivalent, to scaling the positron charge or the electron charge. Such an approach, in fact, would require a scaling of the positron–nuclear repulsion integrals or of the electron-nuclear attraction integrals in addition to the scaling done here. Furthermore, a scaling of the positron charge would require a scaling of the electrostatic interaction outside the box, whereas a scaling of the charge of the target electrons would introduce an attractive Coulomb-potential in the outer region. No such scaling of charges was done here and therefore no compensation of scaled charges is required.

To use $f = 1$ products in the standard *ab initio* results of previous R-matrix studies of positron–molecule collisions. As shown below, the results are very sensitive to the choice of f and values of f only slightly bigger than unity yield surprisingly good agreement with existing experiments.

3. Results and discussion

3.1. Low-energy positron scattering from C_2H_2 targets

As mentioned in the Introduction, the present study intends to select gaseous C_2H_2 as a benchmark system for an extended comparison of methods. Some of the earlier work on this molecule, both for positron and electron

scattering studies, has been carried out by some of the present authors [24–26]. Therefore, the present work employs the same molecular geometry to describe the equilibrium structure of the target, the same quality of Hartree-Fock basis set and, whenever necessary, the same value of the dipole polarizability coefficients for the long-range polarization potential employed in the previous studies [24–26].

The numerical convergence of the SCE has been carefully checked both on the multipolar expansion of the potential ($l_{max} = 30$) and on the number of partial waves describing the scattering e^+/e^- particle.

In the R-matrix calculations for electron and positron scattering we have used the DZP basis set of Dunning and coworkers, an R-matrix box of a radius of $10a_0$ and the continuum basis set of Faure et al. optimized for a box size of $12a_0$ [35]. We have taken the equilibrium geometry ($r_{CC} = 1.208$ Å and $r_{CH} = 1.058$ Å) optimized with the Hartree-Fock method using this basis set. For the positron-scattering calculations using the enhancement factor, we have empirically found a factor $f = 1.004$ by comparing the calculating integral cross section with the experimental results. Differential cross sections were calculated using the program POLYDCS [41].

We report in Fig. 1 the elastic (rotationally summed) integral cross sections for positron scattering, comparing various theoretical results with experiments from Sueoka and Mori [42] The earlier computations from Carvalho et al. [10] are also given in the figure. The following considerations could be made from a perusal of the results reported:

1. The calculations at the static level, carried out with the same basis set and target description, provide the same results when using the SCE and the R-matrix treatment: both curves are given in the lower part of the figure and are essentially coincident, which is a good test for the two different scattering codes.

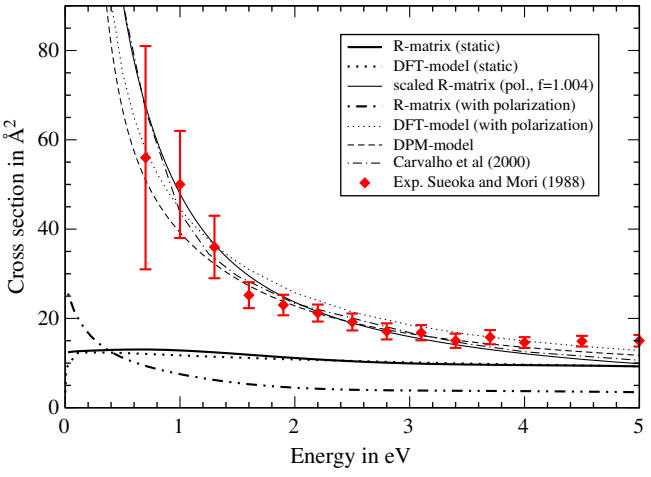

Fig. 1. Integral cross sections for positron–C_2H_2 scattering using various theoretical methods. The experimental results of Sueoka and Mori [42] and the calculations of Carvalho et al. [10] are also given.

2. When correlation–polarization forces are included, we see a dramatic change in the size and behavior of the cross sections obtained within the SCE approach and a remarkable agreement with the experiments down to very low collision energies.
3. The use of the DFT and DPN approximations for V_{pcp} potential yield results which are in very good agreement with each other and in good accord with the experiments. The values of the DPM cross sections are consistently smaller than the DFT data especially around 1 eV and below. However, this difference keeps well below the experimental cross section in the considered energy range.
4. The *ab initio* inclusion of polarization effects within the R-matrix calculations using the SP model is seen, on the other hand, to be still far from convergence although it does give an upturn in the cross section dependance on collision energy near threshold. It is thus clear that the use of configuration interaction methods for treating correlation effects in positron scattering requires a much more extensive inclusion of additional states in order to be able to reproduce the experimental findings.
5. The introduction of the empirical enhancement factor into the R-matrix method markedly improves the agreement with experiments of the calculated cross sections at all energies. Compared with DFT and DPM calculations the RM cross sections are now slightly larger at low energies and slightly smaller at higher energies, although they display the correct energy dependence.

If we now turn to the angular distributions from elastic scattering processes, the results of Fig. 2 report the behavior from the calculations using the DPM model within the SCE treatment of the scattering problem. The two panels of figure report the differential cross sections (DCS) over a broad range of collision energies; the lower panel shows their values at higher energies from 4.0 to 10.0 eV, while the upper panel reports the same quantities down to 0.5 eV. The general trend of all angular distributions remains fairly similar at all energies and indicates the presence of an intensity "dip" that moves to lower angles as the energy increases. Thus, it is only a shallow minimum in the DCS values beyond 130° at 0.5 eV while it moves down to 30° and becomes more marked by the time the collision energy goes up to 10 eV.

The DCS calculated using the R-matrix method via the SP-model, with and without enhancement factor, are given Fig. 3. The results using the SP-model without the enhancement factor are given by thick lines and do not show a strong forward peak. The calculations with an enhancement fact, as in the DPM calculations, show a strong forward peak. Indeed it would appear that at scattering energies above 1 eV the smaller cross sections given by the RM calculations are caused by their underestimation of the strong forward peak.

All computed cross sections turn out to be characterized by a large forward peak and appear to converge to a

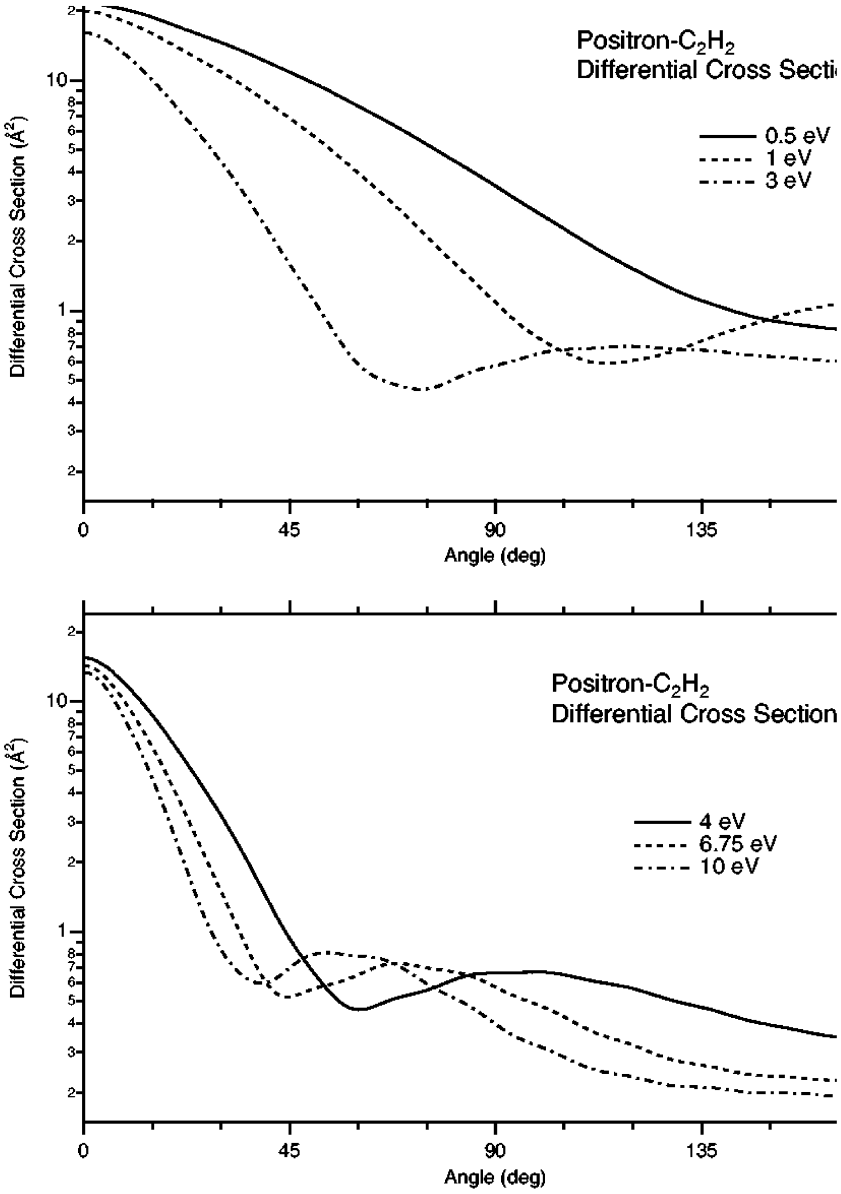

Fig. 2. Computed $e^+ - C_2H_2$ elastic differential cross sections using the DPM modelling of correlation forces. See text for details.

similar limiting value for all energies considered. In other words, the dominance of the $l = 2$ Legendre polynomial, which is associated with the dipole polarizability coefficient, shows up in the angular shape of the DCS at small angles and in the energy dependence of a sort of "magic" angle in the angular distributions.

For the R-matrix calculations including the enhancement factor, the value $f = 1.004$, has been used as a result of optimizing the integral cross sections discussed before. The corresponding results in Fig. 3 are given by thin lines: as mentioned before, the inclusion of the enhancement factor introduces a much more marked forward peaks at all energies. Furthermore these DCS are also showing a minimum which moves to lower angles at increasing energy, as found by the DPM results of Fig. 2. At energies above 4 eV, however, a second minimum appears, which is not observed in the DPM calculations.

Differential cross section for C_2H_2 have also been calculated by Carvalho et al. [43] and measured by Kauppila et al. [44]. The angular distributions in both works are showing strong forward peaks, in agreement with both the DPM calculations of Fig. 2 and the R-matrix calculations with the enhancement factor in Fig. 3.

3.2. Electron scattering from gaseous C_2H_2 targets

As mentioned before, one of the objectives of the present work was to revisit the quantum observables associated with scattering electrons for processes involving the same target, the C_2H_2 molecule, in order to compare the

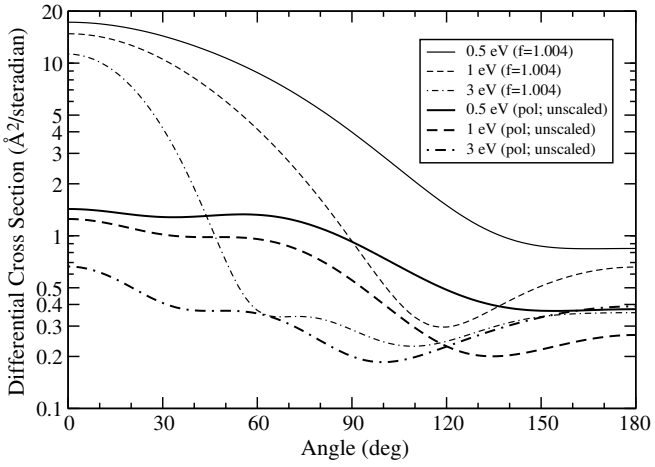

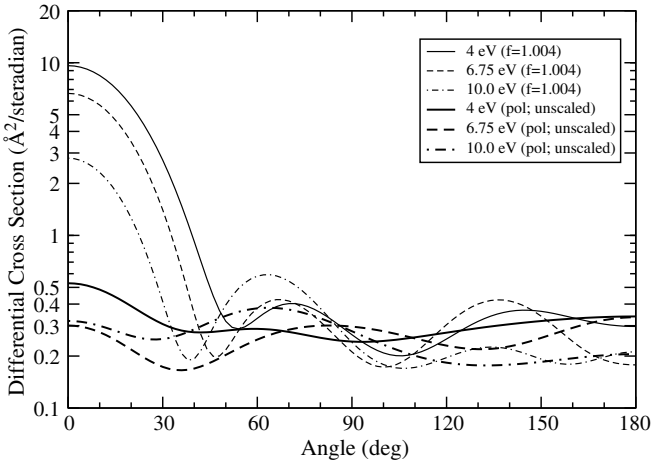

Fig. 3. $e^+ - C_2H_2$ elastic differential cross sections calculated with the R-matrix method using the SP-model with (thin lines) and without (thick lines) using the enhancement factor ($f_{enh} = 1.004$).

performances of different as well as to investigate the differences with the previous comparison carried out for positron–C_2H_2 scattering attributes.

The results reported by Fig. 4 therefore present the calculations at the exact static + exchange level carried out within the SCE expansion but treating both the Static and the exchange potentials as exact contributions since the latter was introduced as a discrete, converged expansion over a separable, additional basis set: for details see our discussion given in reference [45]. The dotted and dash-dotted curves reported by Fig. 4 clearly show the very good numerical agreement exhibited by the SCE and RM methods at the SE level of modelling: thus, these data further confirm the internal reliability of the two approaches in describing e^+/e^- scattering processes.

The inclusion of correlation–polarization forces, both within the SCE-DFT and RM approaches, is reported by the dashed and solid curves, respectively. Here again, the two treatments exhibit reassuring agreement and similarities: the location of the open-channel (shape) resonance feature falls between 2.2 and 2.5 eV, the overall size of the cross sections is also rather similar over the whole range

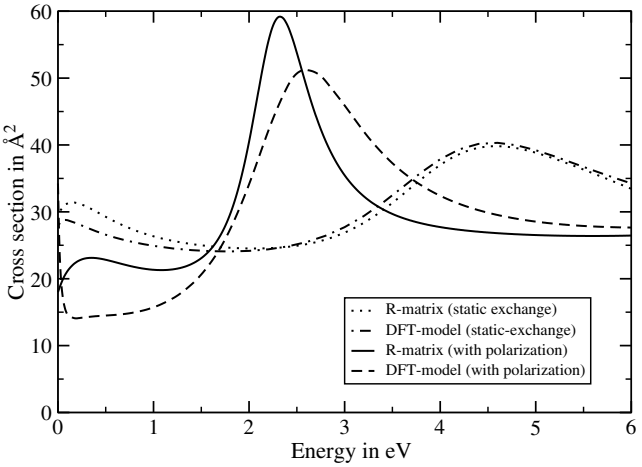

Fig. 4. Electron scattering: computed symmetry components of the elastic integral cross sections (ICS) for electron scattering (upper panel) and a comparison of total ICS obtained either using the DFT correlation polarization model (solid line) or the static + exchange method only (dashes).

of energies and both curves fall out asymptotically to a very similar high-energy value. The threshold behavior, on the other hand, exhibits marked differences very close to zero energies, although both methods would require further numerical tests within that region before anything could be decided on the origin of the discrepancies.

Another interesting set of comparisons is reported by the data shown in the three panels of Fig. 5: we see there the behavior of computed and experimental differential cross sections as a function of collision energies and for three different values of the scattering angles. The top panel refers to $\vartheta = 40^\circ$, the middle panel to $\vartheta = 60^\circ$ and the bottom one to $\vartheta = 90^\circ$, The solid lines refer to the R-matrix calculations while the dashed curves report the SCE-DFT calculations. The experimental data of Kochem et al. are from [46].

We clearly see again that the treatment of correlation effects for electron scattering processes are easier to model *ab initio* within the R-matrix approach than their treatment for positron scattering attributes: the RM results are fairly similar to the DFT calculations without having to introduce any enhancement factor. Furthermore, both computational models follow reasonably well the experimental findings, especially for the case of the DFT results while the RM results turn out to be slightly larger in the energy region of the shape resonance. Both methods, however, reproduce well the general energy dependence of the measured cross sections.

4. Present conclusions

In the present work we have tried to analyze in some detail the relative performances of different computational treatments for obtaining low-energy scattering observables (integral cross sections and angular distributions in the

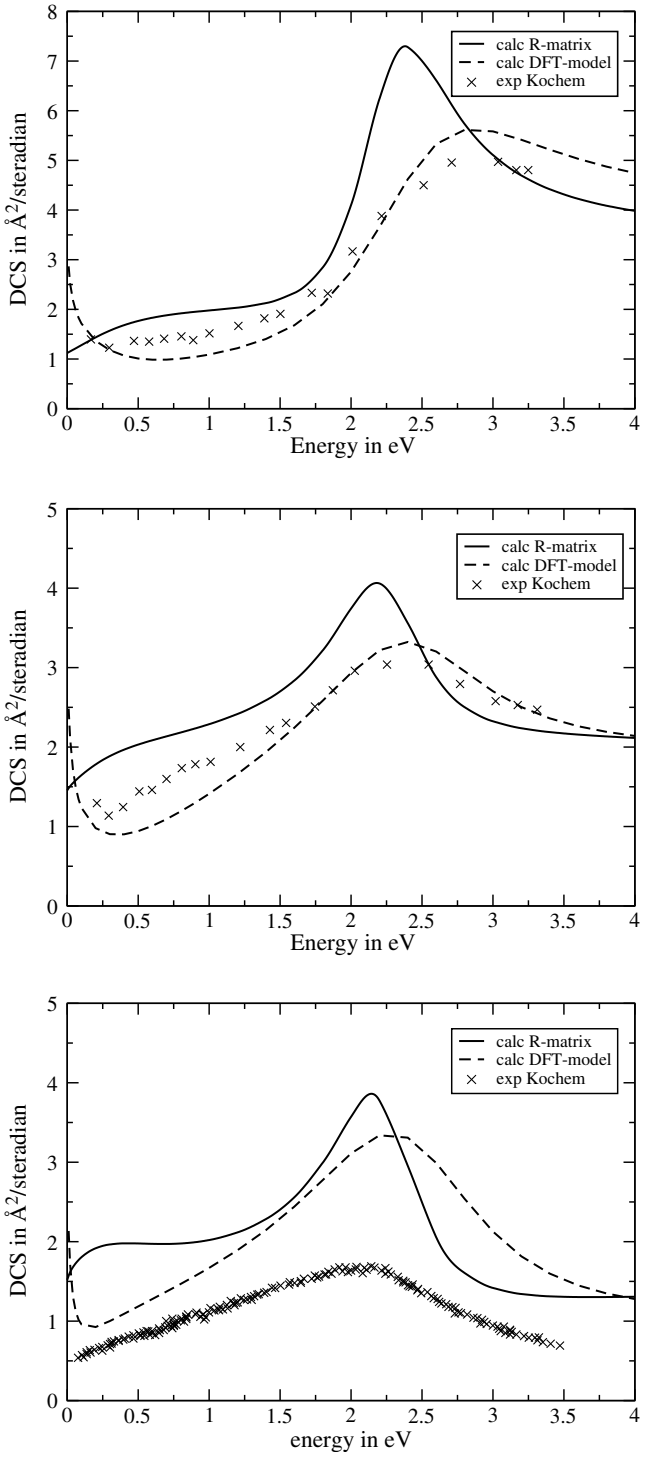

Fig. 5. Computed $e^- - C_2H_2$ angular distributions over the location of the shape resonance energy and for three different angular values ($\theta = 40$, 60 and 90° from top to bottom panel). Experiments are from [46].

elastic channels) associated with both positron and electron low-energy collisions with a specific polyatomic target: the C_2H_2 molecule at its equilibrium geometry.

In particular, we have first made sure that both methods are comparable when the interaction forces are artificially simplified to be given either by Static interaction only (for e^+ scattering) of by static + exchange interactions (for e^- scattering): the present results clearly show that indeed both sets of codes produce the same integral elastic (rotationally summed) cross sections in spite of their implementing very different computational procedures.

The next step has been to add within both treatments the effect of correlation–polarization forces as implemented within each code.

The results which compare our findings with experiments in the case of the positron scattering show that the DFT/DPM modelling of correlation forces, neither of which are entirely *ab initio* are both able to yield remarkable agreement with observed quantities, while the *ab initio* RM approach moves in the correct direction but manages to reach the same good agreement only when an empirical enhancement factor is included. Thus the RM approach still requires further work for positron scattering studies on the treatment of correlation–polarization effects in order to achieve an acceptable level of convergence.

The corresponding analysis of computed angular distributions largely confirms the above findings. The two methods produce very similar results only when the empirical enhancement factor is employed within the RM calculations.

Finally, the comparison between scattering attributes, as obtained by the two methods analysed in the present work, has been extended to electron collisions from the same molecular target. The results reported by Figs. 4 and 5 indeed confirm the methods' reliability at the SE level but also indicate the quality of the RM outcome when electron projectiles are considered: both methods now yield similar results without using an enhancement factor within the RM calculations. In general, however, the DFT angular distributions appear to follow more closely the experimental data over a broad range of energies.

In conclusion, the present benchmark calculations have allowed us to attain the following, interesting results:

1. That the existing implementations of the R-matrix and of the SCE-DFT approaches for treating e^+/e^- electronically elastic scattering off polyatomic targets provide essentially the same results when using the same interaction potentials.
2. That the two codes model very differently the further inclusion of correlation–polarization forces and therefore show up at this level their differences of behavior.
3. That the DFT approach is found to be able to model such effects in ways which turn out to reproduce very well experimental results for positron and for electron scattering.
4. That the RM approach shows faster CI convergence in the case of electron scattering data while still requires much larger expansion treatments in the case of positron scattering, as indicated by its empirical need of including an enhancement factor in the latter case.

We have therefore shown that at least two different approaches to multichannel scattering methods which provide observables for polyatomic targets can be reliably

employed in the future to yield complementary information for the ever increasing range of polyatomic gases that are being experimentally analyzed.

Acknowledgements

J.F., J.T. and K.L.B. acknowledge funding from both EPSRC and the Royal Society through their India–UK exchange program. J.F. thanks the EIPAM network of the European Science Foundation (ESF) for the award of a fellowship at the beginning of the present work. F.A.G. further thanks the CASPUR Consortium for the availability of computational time for the present project. This work was also supported by the Robert A. Welch Foundation (Houston, TX) under grant A-1020.

References

[1] e.g. see: M. Charlton, J. Humbertson, Positron Physics, Cambridge University Press, New York, 2001.
[2] C.M. Surko, F.A. Gianturco (Eds.), New Directions in Antimatter Chemistry and Physics, Kluwer Academic Publishers, Dordrecht, 2001.
[3] P.J. Schultz, K.G. Lynn, Rev. Mod. Phys. 60 (1988) 701.
[4] M. Kimura, O. Sueoka, A. Hamada, Y. Itikawa, Adv. Chem. Phys. 111 (2000) 537.
[5] C.M. Surko, G.F. Gribakin, S.J. Buckman, J. Phys. B 38 (2005) R57.
[6] M. Puska, R. Nieminen, J. Phys. F 13 (1963) 333.
[7] e.g. see F.A. Gianturco, T. Mukerjee, Phys. Rev. A 55 (1997) 1044.
[8] T.L. Gibson, J. Phys. B 25 (1992) 1321.
[9] P.G. Burke, K.A. Berrington (Eds.), Atomic and Molecular Processes: an R-matrix approach, Ins. of Phys. Pub., Bristol and Philadelphia, 1993.
[10] C.R.C. de Carvalho, M.T.doN. Varella, M.A.P. Lima, E.P. da Silva, J.S.E. Germano, Nucl. Instr. Meth. B 171 (2000) 33.
[11] e.g. see F.A. Gianturco, A. Jain, Phys. Rep. 143 (1986) 347.
[12] E.S. Chang, U. Fano, Phys. Rev. A 6 (1972) 173.
[13] F.A. Gianturco, R. Curik, N. Sanna, J. Phys. B: At. Mol. Opt. Phys. 33 (2000) 2705.
[14] A. Jain, F.A. Gianturco, J. Phys. B 24 (1991) 2387.
[15] J. Arponen, E. Payenne, Ann. Phys. NY 121 (1979) 343.
[16] E. Boronski, R.M. Nieminen, Phys. Rev. 34 (1986) 3820.
[17] T.L. Gibson, J. Phys. B 23 (1990) 767.
[18] R.R. Lucchese, F.A. Gianturco, P. Nichols, T.L. Gibson, in: C. Surko, F.A. Gianturco (Eds.), New Directions in Antimatter Chemistry and Physics, Kluwer Academic, Dordrecht, 2001, p. 475.
[19] F.A. Gianturco, T.L. Gibson, P. Nichols, R.R. Lucchese, T. Nishimura, Radiat. Phys. Chem. 68 (2003) 673.
[20] F.A. Gianturco, P. Nichols, T.L. Gibson, R.R. Lucchese, Phys. Rev. A 72 (2005) 032724.
[21] A. Szabo, N. Ostlund, Modern Quantum Chemistry, Dover, New York, 1996, p. 158.
[22] A. Bouferguene, I. Ema, C.A. Weatherford, Phys. Rev. A 59 (1999) 2712.
[23] e.g. see N.F. Lane, Rev. Mod. Phys. 52 (1980) 29.
[24] A. Occhigrossi, F.A. Gianturco, J. Phys. B 36 (2003) 1383.
[25] T. Nishimura, F.A. Gianturco, Nucl. Instr. and Meth. B 221 (2004) 24.
[26] F.A. Gianturco, J. Comp. Theor. Chem. 5 (2006) 543.
[27] L.A. Morgan, J. Tennyson, C.J. Gillan, Computer Phys. Comms. 114 (1998) 120.
[28] C.J. Noble. The ALCHEMY Linear Molecule Integral Generator. DL/SCI/TM33T Daresbury Laboratory Technical Memorandum, 1982.
[29] L.A. Morgan, C.J. Gillan, J. Tennyson, X. Chen, J. Phys. B: At. Mol. Opt. Phys. 30 (1997) 4087.
[30] J. Tennyson, J. Phys. B: At. Mol. Phys. 19 (1986) 4255.
[31] G. Danby, J. Tennyson, J. Phys. B: At. Mol. Opt. Phys. 23 (1990) 1005.
[32] K.L. Baluja, R. Zhang, J. Franz, J. Tennyson, J. Phys. B: At. Mol. Opt. Phys. 40 (2007) 3515.
[33] J. Tennyson, J. Phys. B: At. Mol. Opt. Phys. 29 (1996) 1817.
[34] J. Franz, K.L. Baluja, R. Zhang, J. Tennyson, Nucl. Instr. and Meth. B 266 (2008) 419.
[35] A. Faure, J.D. Gorfinkiel, L.A. Morgan, J. Tennyson, Comp. Phys. Comms. 144 (2002) 224.
[36] A. Takatsuka, S. Ten-no, Bull. Korean Chem. Soc. 24 (2003) 859.
[37] Y. Itikawa, Theo. Chem. Acc. 105 (2000) 123.
[38] J.D. Gorfinkiel, J. Tennyson, J. Phys. B: At. Mol. Opt. Phys. 37 (2004) L343.
[39] J.D. Gorfinkiel, J. Tennyson, J. Phys. B: At. Mol. Opt. Phys. 38 (2005) 1607.
[40] G. Danby, J. Tennyson, J. Phys. B: At. Mol. Opt. Phys. 24 (1991) 3517.
[41] N. Sanna, F.A. Gianturco, Comput. Phys. Commun. 114 (1998) 142.
[42] O. Sueoka, S. Mori, J. Phys. B At. Mol. Opt. Phys. 22 (1989) 963.
[43] C.R.C. de Carvalho, M.T. do Varella, M.A.P. Lima, E.P. da Silva, Phys. Rev. A 68 (2003) 062706.
[44] W.E. Kauppila, C.E. Kwan, D.A. Przybyla, T.S. Stein, Nucl. Instr. and Meth. B 192 (2002) 162.
[45] F.A. Gianturco, T. Stoecklin, J. Phys. B 27 (1994) 5903.
[46] K.H. Kochem, W. Sohn, K. Jung, H. Ehrhardt, E.S. Chang, J. Phys. B: At. Mol: Opt. Phys. 18 (1985) 1253.